Alfvénic phenomena triggered by resonant absorption of an O-mode pulse

F. S. Tsung, G. J. Morales, and J. Tonge
Department of Physics and Astronomy, University of California, Los Angeles, California 90095

(Received 6 October 2006; accepted 29 January 2007; published online 5 April 2007)

A simulation and modeling study is made of the nonlinear interaction of an electromagnetic pulse, in the O-mode polarization, with a magnetized plasma having a cross-field density gradient. For small amplitudes, the pulse propagates up to the cutoff layer where an Airy pattern develops. Beyond a certain power level, the ponderomotive force produced by the standing electromagnetic fields carves density cavities. The excess density piled up on the side of the cavities causes secondary, field-aligned plasma resonances to arise. Strong electron acceleration occurs due to the short scale of the secondary resonant fields. The fast electrons exiting the new resonant layers induce a return current system in the background plasma. This generates a packet of shear Alfvén waves of small transverse scale and increasing frequency. The results provide insight into microscopic processes associated with a recent laboratory investigation in which large-amplitude Alfvén waves have been generated upon application of high-power microwaves [B. Van Compernolle *et al.*, Phys. Plasmas **13**, 092112 (2006)]. © *2007 American Institute of Physics*. [DOI: 10.1063/1.2711428]

I. INTRODUCTION

The excitation of low-frequency electromagnetic waves in the band below the ion cyclotron frequency (i.e., $\omega < \Omega_i$) by pump waves having frequency on the order of the electron plasma frequency (i.e., $\omega_0 \cong \omega_{pe}$) has been a subject of continued interest in ionospheric heating studies.[1–3] In essence, the problem involves issues of multiscale coupling, which is a topic of contemporary interest[4] in a broad range of plasma applications. In the ionospheric context, a variety of mechanisms have been considered to bring about the coupling across the disparate frequency scales. Some mechanisms are based on parametric instabilities[5,6] while others involve modifications of the zero-order plasma parameters.[7–9]

Although an extensive theoretical literature exists on this subject and large field experiments[10–12] have been deployed worldwide, until recently there has been a lack of basic laboratory experiments and computer simulation studies of related phenomena. The reason why the laboratory and simulation studies have not been forthcoming is that experimental and computational tools capable of sampling the different time scales have not been available. With the advent of the Large Plasma Device (LAPD-U) operated by the Basic Plasma Science Facility (BaPSF)[13] at the University of California, Los Angeles (UCLA), it is now feasible to explore, under controlled conditions, the cross-coupling between electron plasma-wave physics and Alfvénic interactions. Recent experiments[14] have demonstrated conclusively that shear Alfvén waves of substantial amplitude are excited when a magnetized plasma is irradiated with a high-power microwave pulse.

The situation with particle-in-cell (PIC) simulations of this type of problem parallels the laboratory developments. Recently, the computational power reached a level that permits the investigation of Alfvénic phenomena within turnaround times that make exploratory studies practical. It is the purpose of this paper to use PIC-based studies to identify the microscopic processes underlying the laboratory results. While at this stage the properties of the Alfvén waves generated have been mapped in great detail in the LAPD-U experiments,[14] the underlying microscopic processes have not yet been isolated. The results of the present study provide insight as to what is the relevant nonlinear physics and indicate what experimental tools must be deployed for their identification in future campaigns.

The highlight of the present study is the identification of secondary, field-aligned resonances having short parallel scale. It is these short-scale electric fields that generate the fast electrons that act as moving antennas to excite shear Alfvén waves. The secondary resonances arise from the density pileup at the edge of cavities formed by the ponderomotive force produced by the primary fields of the O-mode pulse.

The paper is organized as follows. Section II explains the simulation model and the linear propagation features. Section III A catalogues the various nonlinear processes identified in the PIC simulation and interprets them with a fluid-based analytical model. Section III B details the properties of the radiated Alfvén waves. Conclusions are presented in Sec. IV.

II. SIMULATION MODEL

A schematic of the geometry of the problem considered is shown in Fig. 1. A uniform magnetic field B_0 points along the z direction while the plasma density $n_0(x)$ varies in the transverse x direction (indicated by the gray-black shaded region). A source of electromagnetic waves having frequency ω_0 is located on the low-density side ($x=0$), with its center at the origin of the z axis. The source emits a pulse of radiation with a characteristic pulse length comparable to the ion gyroperiod, i.e., $2\pi/\Omega_i$. The other Cartesian coordinate, y, mutually perpendicular to (x,z) and pointing into the page, is

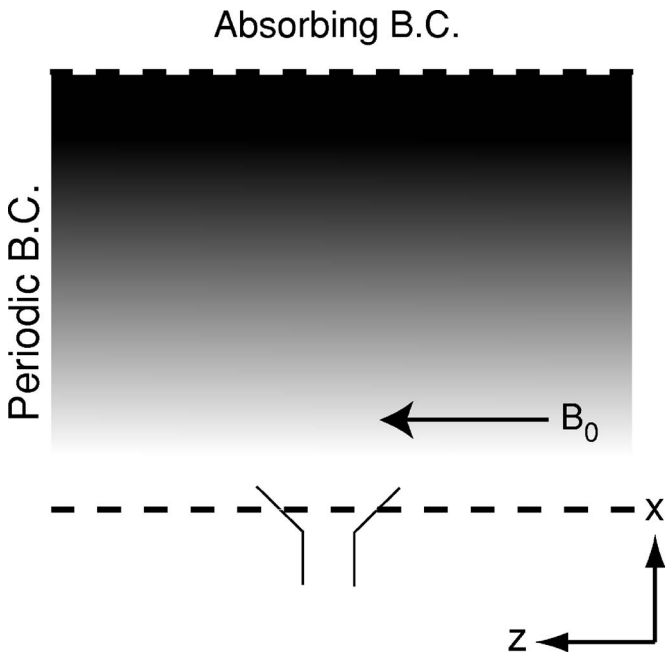

FIG. 1. Schematic of geometry considered. A uniform magnetic field B_0 points along the z direction and the plasma density varies in the transverse x direction. Dark indicates high density and light low density. A source centered at $z=0$ on the low-density side, $x=0$, emits an O-mode pulse at frequency ω_0. The other coordinate, y, into the page, is ignorable.

ignorable. The electromagnetic pulse has finite extent in the z direction and its electric field vector is parallel to the z direction, i.e., it is an O-mode. For low power levels, the pulse is predicted to propagate up to the O-mode cutoff layer, i.e., where $\omega_0=\omega_{pe}(x)$. The pulse reflects without absorption because the O-mode does not experience a linear resonance. The distance between the reflection layer and the source is determined by the density scale length L_N. For large power levels, nonlinear processes trigger the emission of shear Alfvén waves having small transverse scale across B_0 (the z direction). The goal of this study is to identify these nonlinear processes with the aid of a particle-in-cell (PIC) simulation code, complemented by an analytical model.

The code used in this investigation is based on a code (OSIRIS) originally developed to study laser-plasma interactions.[15] Over the past few years, this code has been appropriately extended to permit the exploration of Alfvénic phenomena. In a previous study, the modified code has been used to investigate the expansion of a magnetized supersonic plume,[16] and to elucidate processes related to laser ablation experiments.[17] More recently, the code has been used[18] to investigate the propagation properties, in the inertial and kinetic regimes, of shear and compressional Alfvén waves excited by a boundary source. From extensive checks leading to these previous investigations, it has been demonstrated that the code correctly describes the expansion of fast electrons in magnetized plasmas, as well as all the characteristic features of Alfvénic signals. Both of these elements are essential to the present investigation.

The code is electromagnetic and follows the self-consistent, relativistic orbits of magnetized electrons and ions. The results presented here are run in 2-1/2 dimensions (two spatial dimensions and three velocity directions) using 64 processors in the Dawson cluster at UCLA. As is indicated in Fig. 1, for this study the code is run with absorbing boundaries along the x direction and periodic boundaries along the z direction. The length of the computational box along the z direction is chosen much longer than the transverse direction in order to resolve the filamentary structure of shear Alfvén modes.[19,20] The results reported correspond to time scales shorter than the time it takes for the signal to wrap around the periodic box. Thus, the boundary conditions play no role in the results shown here.

The plasma and wave parameters are chosen to approximate the conditions in the LAPD-U experiment,[14] but are also representative of a wide variety of situations. The plasma is taken to be initially cold, with the magnetic field strength resulting in an electron gyrofrequency $\Omega_e=0.4\omega_0$ (in the LAPD-U experiment this coefficient can range from 0.278 to 0.43). The typical scaled density length is $k_0L_N=105$, where $k_0=\omega_0/c$ with c the speed of light. The ion to electron mass ratio is $M/m=20$. This is a relatively small value, but it has been found to be adequate in separating the relevant frequency scales while permitting computing runs with practical turnaround times.

The spatial dependence of the initial plasma density is given by

$$n_0(x)=n_l\left(1+\frac{x}{L_N}\right), \tag{1}$$

with a typical edge density $n_l=0.7n_c$, where n_c is the cutoff (critical) density corresponding to ω_0. Note that the density gradient scale, normalized to the cutoff density, is given by L_N/n_l.

The transverse shape of the injected electromagnetic pulse at $x=0$ is given by $g(z)=\exp(-z^2/L^2)$, with L the effective width at the source. The temporal shape of the pulse is $[T(t/\tau_0)+T(2\tau_0-t/\tau_0)]$, where the function $T(\tau)$ is defined as $T(\tau)=(10\tau^3-15\tau^4+6\tau^6)$. The characteristic pulse width τ_0 is typically on the order of one ion gyroperiod. The range of power levels over which the phenomena reported here have been explored corresponds to injected peak vacuum electric fields E_0 satisfying $v_{os}/v_A\leq 4$, where $v_{os}=eE_0/(m\omega_0)$ and v_A is the Alfvén speed at the cutoff layer. These values are comparable to those used in experiments.[14]

The capability of the code to simulate the propagation of electromagnetic pulses in magnetized plasmas is illustrated in Fig. 2. To accentuate the nontrivial propagation characteristics, a source with narrow extent ($L=1.0c/\omega_0$) along the z direction is activated. The narrow extent of the source implies that a broad spectrum of modes having wave numbers oblique to the density gradient is radiated. Each Fourier component radiated exhibits a different group velocity vector and accordingly reflects at densities lower than predicted by the condition $\omega_0=\omega_{pe}(x)$. The wide radiation pattern obtained from the PIC simulation for a low power ($v_{os}/v_A=0.2$), O-mode pulse, is illustrated in Fig. 2. The z axis is along the vertical direction while the x axis is along the horizontal. It should be noted that in Fig. 2 the z direction is scaled to the ion skin depth c/ω_{pi0} (at the reflection layer), while the x

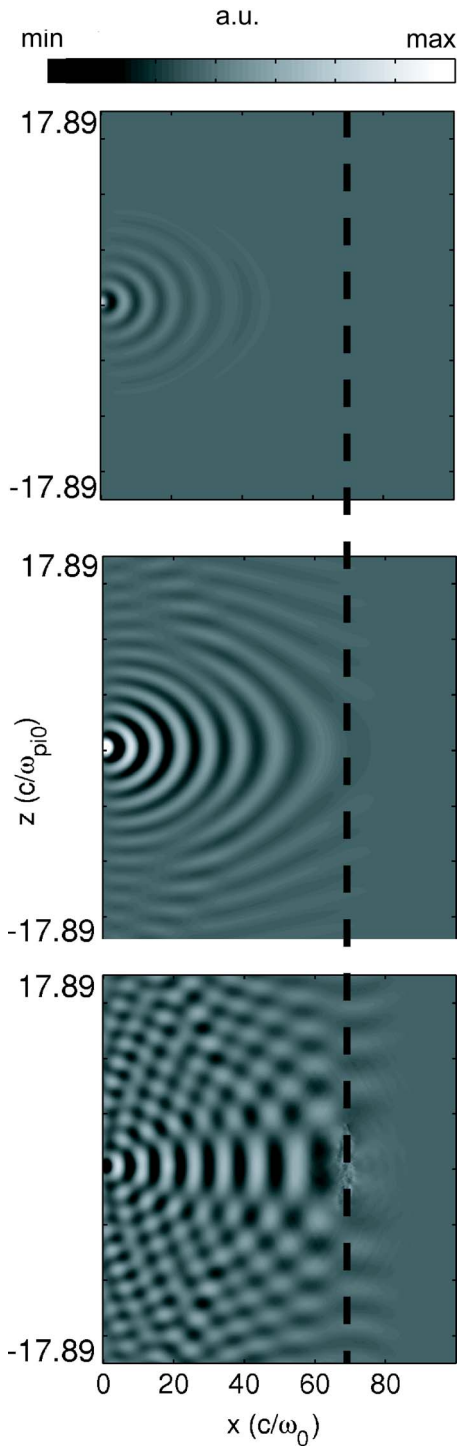

FIG. 2. Radiation pattern of a narrow source in a linear regime with $L=1.0c/\omega_0$. Gray-scale spatial contours in the (x,z) plane of the instantaneous component of wave magnetic field in the y direction, B_y, for different times. Top, $\omega_0 t=114$; middle, $\omega_0 t=228$; bottom, $\omega_0 t=457$. Largest positive value is white and largest negative value is black. The z direction (vertical) is scaled to ion skin depth and the x direction (horizontal) to electron skin depth.

direction is scaled to the electron skin depth c/ω_0. The quantity displayed is the spatial contour of the instantaneous value of the component of the wave magnetic field along the ignorable y direction, B_y. In the gray scale used, white corresponds to the largest positive value and black to the largest negative value. The panels correspond to three different times after the source is turned on ($t=0$). The top panel shows the early stage ($\omega_0 t=114$) when the pulse penetrates into the plasma across the magnetic field. The middle panel at $\omega_0 t=228$ corresponds to the arrival of the spreading front of the pulse to the reflection layer, while the bottom panel at $\omega_0 t=457$ exhibits the nearly steady-state pattern. At this late stage, partially standing waves are formed across, as well as along, the confinement magnetic field. In the three panels of Fig. 2, the dark dashed line indicates the location where $\omega_0=\omega_{pe}(x)$. It is observed from Fig. 2 that some components of the electromagnetic pulse reflect at lower densities, as expected, and result in a relatively wide beam returning to the plasma edge.

III. NONLINEAR BEHAVIOR

A. Profile modification

In contrast to the narrow source used in generating Fig. 2, now a source having a moderate width ($L=15c/\omega_0$), comparable to that used in the LAPD-U experiments, is considered. In this case, the electromagnetic beam remains well-collimated as it crosses the confinement magnetic field upon entry and subsequent reflection from the plasma. This implies that in this case, a well-defined standing-wave structure can be formed between the source region and the reflection layer. Figure 3 displays the essential elements of the linear plasma response in the low-power regime obtained with a source strength of $v_{os}/v_A=.03$ at a scaled time $\omega_0 t=585$. This corresponds to a time after which the signal completes a full transit and a near steady-state pattern is formed.

Figure 3(a) shows contours of the ion density in the (x,z) plane. In this panel, the z direction is horizontal and the x direction is vertical. It is found that at this low-power level there are no perceptible modifications of the density profile. The vertical dashed lines in Fig. 3(a) indicate cuts, at fixed z locations, along which phase-space information is sampled, as shown in Figs. 3(b) and 3(c). The cuts correspond to symmetric locations ($z=\pm 4.47c/\omega_{pi0}$) to the right and left of the center of the O-mode beam.

Figures 3(b) and 3(c) provide a snapshot of the modulation of the parallel velocity (i.e., the z component) of plasma electrons along the dashed lines indicated in Fig. 3(a). What is displayed in Figs. 3(b) and 3(c) is a mixed phase space, p_z vs x, with momentum scaled to mv_A. In the linear regime sampled, the initially cold electrons are not heated by the electromagnetic wave. Consequently, what is seen in Figs. 3(b) and 3(c) is essentially the oscillatory velocity imparted on the electrons by the z component of the electric field of the O-mode. It should be mentioned that the beam extent along the z direction is such that an electron experiences many reversals in the direction of the O-mode electric field while it is inside the beam footprint. Thus, there is no significant transit-time absorption.[21] Figures 3(b) and 3(c) indicate that at low-power levels, the parallel electric field exhibits an Airy type of pattern across the confinement magnetic field, as is expected.

The nonlinear behavior obtained as the source power level is increased to a value corresponding to $v_{os}/v_A=0.5$ is shown in Fig. 4 for a time $\omega_0 t=583$. The various panels in

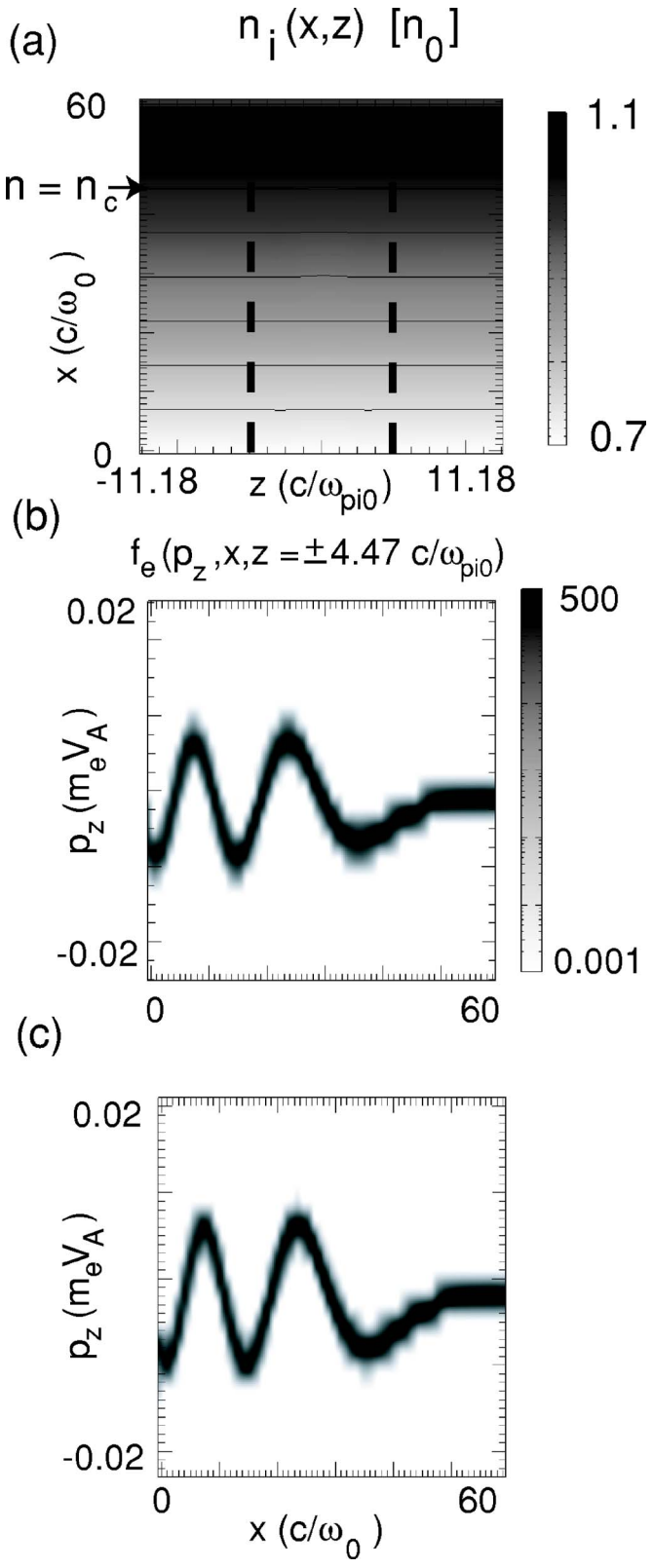

FIG. 3. Linear response at $\omega_0 t=583$ for a wide source with $L=15c/\omega_0$ and $v_{os}/v_A=0.03$; (x,z) directions are as in Fig. 1. (a) Gray-scale contours of ion density. Dark is high and light is low density. Arrow indicates cutoff layer. (b) and (c) are mixed phase-space projections (p_z,x) for electrons along the dashed lines shown in (a). (b) $z=4.47c/\omega_{pi0}$, (c) $z=-4.47c/\omega_{pi0}$. Velocity modulation following characteristic Airy pattern is seen. Momentum is scaled to mv_A.

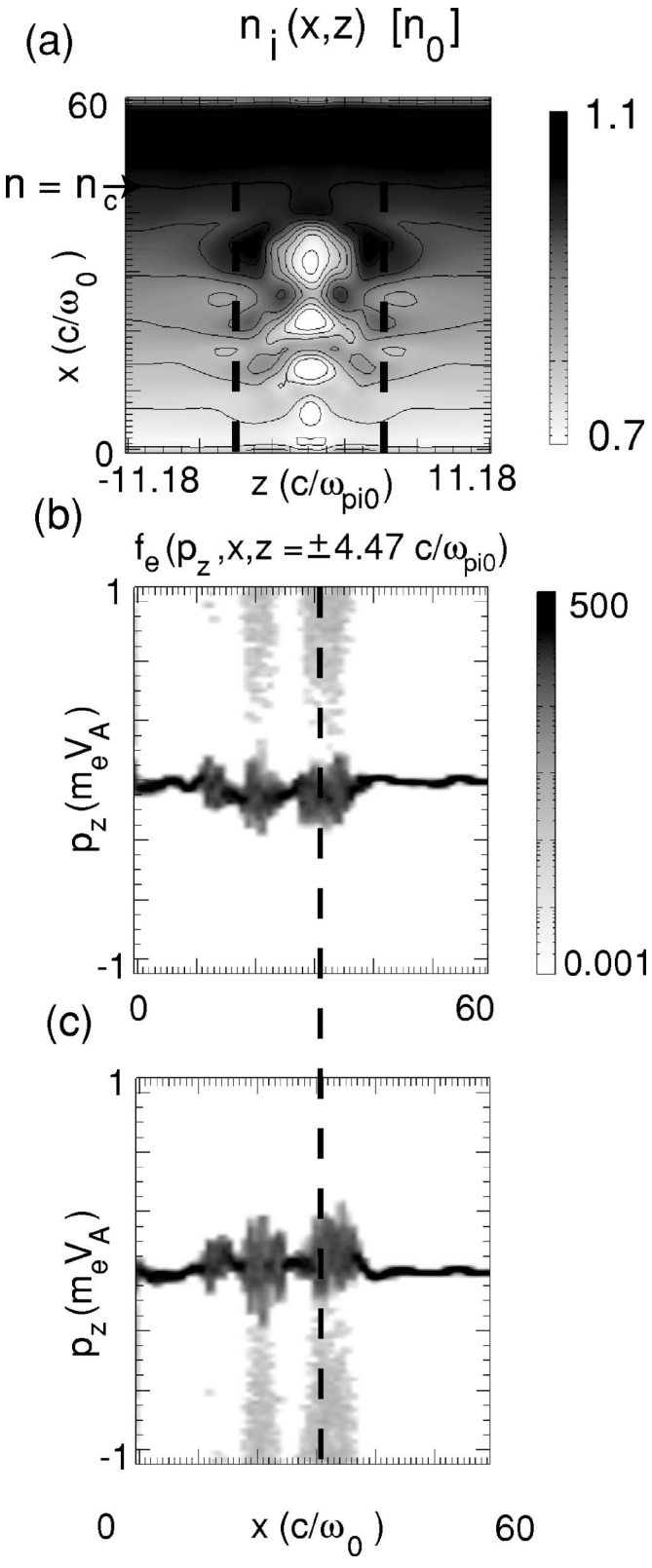

FIG. 4. Nonlinear response at $\omega_0 t=583$ for a wide source with $L=15c/\omega_{pe}$ and $v_{os}/v_A=0.5$. Equivalent to Fig. 3. (a) Density cavities are formed by a standing pattern of O-mode. (b) and (c) Phase-space snapshots show electrons are heated where density cavities are formed and field-aligned fast electron tails exit these regions.

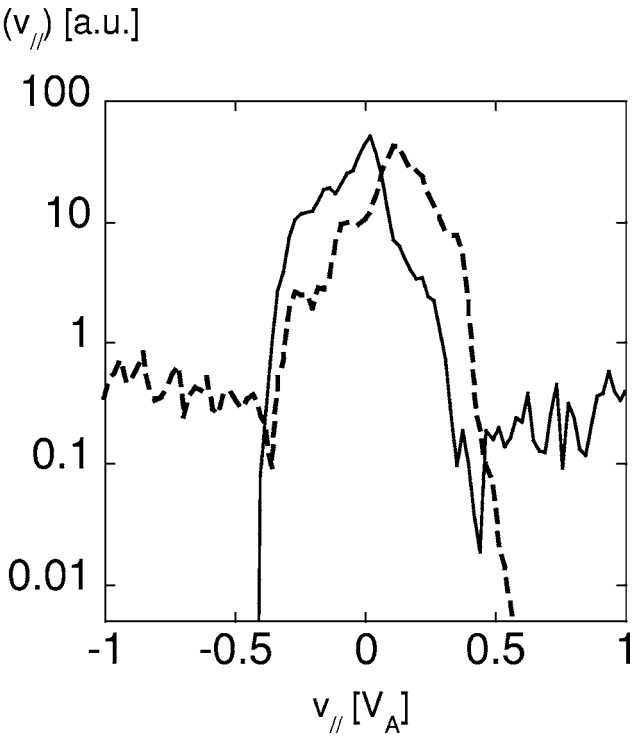

FIG. 5. Parallel (z direction) velocity distribution function (logarithmic scale) of electrons at position $x=31c/\omega_0$ indicated by the dashes in Figs. 4(b) and 4(c). Dashed curve is for $z=-4.47c/\omega_{pi0}$ and solid for $z=4.47c/\omega_{pi0}$. The distribution functions exhibit bulk heating and fast tails. The bulk particles experience a net drift that provides a return current.

this figure are arranged as in the linear case in Fig. 3 and contain equivalent information. It is now seen that Fig. 4(a) exhibits major rearrangements in the plasma density profile. The structures formed consist primarily of density cavities (i.e., depletions) whose centers coincide with the peak values of the square of the parallel electric field of the electromagnetic wave, i.e., $|E_z|^2$. The plasma particles removed to form the cavities spread predominantly along the confinement magnetic field (i.e., the z direction), although a small density compression does develop across the magnetic field.

Figures 4(b) and 4(c) do not show the coherent, Airy type of oscillations seen in the corresponding panels (b) and (c) of Fig. 3. Instead, one observes a broadened pattern with a spatial modulation (in the x direction) approximately corresponding to the square of the parallel electric field. The smearing seen in Figs. 4(b) and 4(c) implies that the electrons have been heated. In addition to the heating, a smaller population of fast electrons is generated. These fast tails are seen to emanate from the regions where the density cavities attain their deepest value. A comparison of Figs. 4(b) and 4(c) indicates that fast electrons emerge symmetrically (along the confinement magnetic field) from the sides of the O-mode beam.

Figure 5 shows the parallel (z direction) velocity distribution function (in logarithmic scale) of electrons at position $x=31c/\omega_0$ indicated by the dashed line in Figs. 4(b) and 4(c). This position corresponds to where the parallel electric field of the O-mode attains its largest value. The two curves in Fig. 5 represent the parallel electron distribution functions at $z=4.47c/\omega_{pi0}$ (solid) and $z=-4.47c/\omega_{pi0}$ (dashed), which again are associated with cuts along the two dashed lines in Fig. 4(a). It is seen in Fig. 5 that the distribution functions exhibit bulk heating and fast tails populated at velocities larger than the oscillatory velocity due to the primary O-mode electric field. It can also be deduced from Fig. 5 that the bulk (slow) electrons experience a net drift in a direction opposite to that in which the fast tails move, i.e., the bulk electrons carry a return current that compensates for the current injected by electrons in the fast tail. It is shown later in Sec. III B that such a current system is related to a shear Alfvén wave.

To obtain a better understanding of the early stage of the nonlinear profile modification and to independently corroborate the results of the PIC code, it is useful to develop an approximate analytical description of the phenomena. For the early stage during which the plasma has not yet been heated, a fluid description is useful. In this spirit, the high-frequency O-mode imparts on the electrons a low-frequency force, the ponderomotive force, which acts primarily along the confinement magnetic field. Because at early times there is not yet a significant electron pressure, the ponderomotive force must be balanced by an electrostatic potential given by

$$\phi(x,z)=\left(\frac{m}{2e}\right)\langle\tilde{v}_e^2\rangle, \tag{2}$$

where

$$\langle\tilde{v}_e^2\rangle=\left(\frac{1}{2}\right)\left(\frac{eE}{m\omega_0}\right)^2, \tag{3}$$

with E the complex amplitude of the parallel electric field of the O-mode, and e the quantum of charge.

The electrostatic field holding back the cold electrons pushes the ions, which on the short time scale behave as unmagnetized. Thus, the ion velocity v_i and the ion density n_i are determined by the equation of motion and the continuity equation, respectively,

$$M\frac{d}{dt}\vec{v}_i=-e\,\nabla\,\phi, \tag{4}$$

$$\frac{\partial}{\partial t}n_i=-\nabla\cdot(n_i\vec{v}_i). \tag{5}$$

An equation that describes the early stage of profile rearrangement is obtained by linearizing Eqs. (2)–(5),

$$\frac{\partial^2}{\partial t^2}n_i=\left(\frac{m}{2M}\right)\nabla\cdot[n_0(x)\,\nabla\langle\tilde{v}_e^2\rangle], \tag{6}$$

and where, consistently, the amplitude of the electric field is approximated by its value for the unperturbed density profile represented by Eq. (1). This results in

$$E(x,z)=E_0 g(z)A_i(\zeta), \tag{7}$$

$$\zeta=\left[k_0L_N\frac{n_c}{n_l}\right]^{2/3}\left[\left(\frac{n_l}{n_c}\right)\left(1+\frac{x}{L_N}\right)-1\right], \tag{8}$$

with n_c the density at the cutoff layer and A_i is the usual Airy function. The factor $g(z)$ is the beam profile of the O-mode;

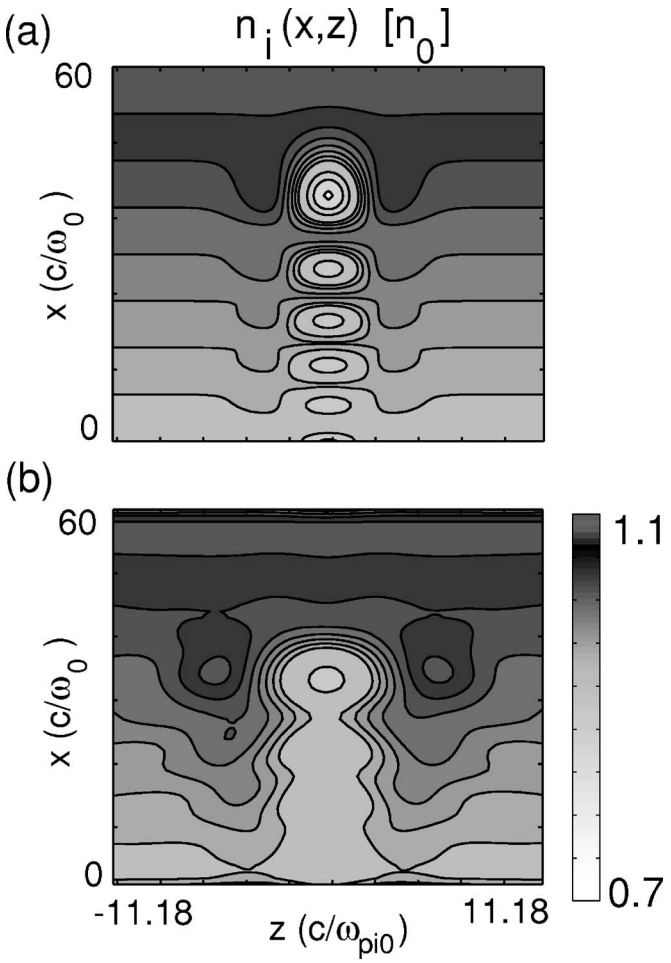

FIG. 6. Gray-scale contours of spatial (x,z) dependence of instantaneous ion density. (a) Density profile modification predicted by Eq. (6). Dark, large density; light, low density. Density depressions centered at the peak values of $|E_z|^2$ are formed. Each depression is accompanied by a density pileup along the confinement magnetic field. (b) Result of PIC simulation shows similar behavior, but modified by plasma heating.

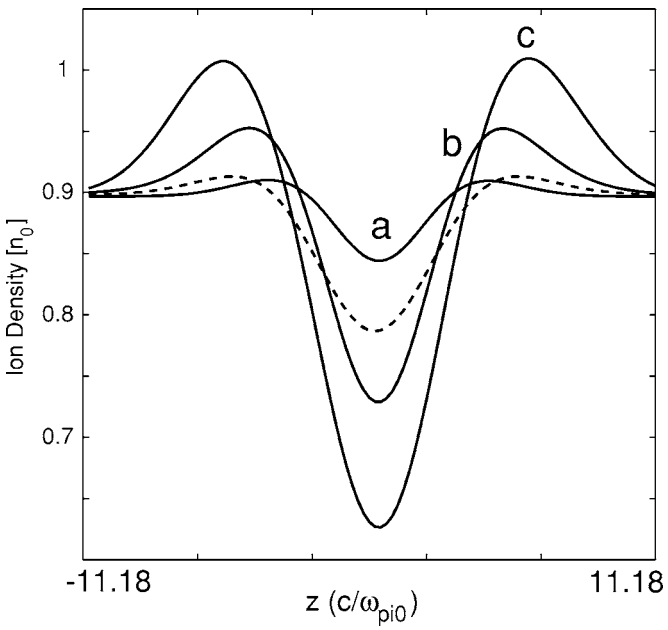

FIG. 7. Axial dependence of the ratio of the modified ion density to the cutoff density, n_i/n_c, along an initially underdense field line. Solid curves are PIC simulation for different times (a) $\omega_0 t=520$, (b) $\omega_0 t=845$, and (c) $\omega_0 t=1300$. Dashed line is the prediction of Eq. (6). PIC results show the development of "density wings" that eventually result in the formation of new resonant layers $(n_i/n_c=1)$ having small scale.

it is approximated by the value specified at the source, i.e., $g(z)=\exp(-z^2/L^2)$.

This model for density modification is appropriate for time scales before large cavities are formed and not much heating occurs. As the density cavities attain a significant level, the neglected terms become important and provide a saturation mechanism for the early secular growth, i.e., $n_i \sim t^2$, obtained from Eq. (6). Also, as the density profile is rearranged, the O-mode waveform deviates from the Airy pattern.

Figure 6(a) illustrates the characteristic profile modification predicted by Eq. (6). This is a contour plot of the dependence of the instantaneous ion density on the z and x coordinates. Dark colors indicate large density and light colors low density. The modified profile consists of density depressions centered at the peak values of $|E_z|^2$. Several cavities are seen because a standing wave is formed between the source and the cutoff layer. Each of the density depressions is accompanied by a corresponding density pileup on its sides, i.e., along the confinement magnetic field. These "density wings" play a key role in electron acceleration and the subsequent excitation of Alfvén waves. For comparison, Fig. 6(b) displays the corresponding density profile obtained in the PIC simulation. Indeed, it is seen in the simulation that the process of density depletion occurs and results in the development of the "density wings" predicted by the model. However, the simulation yields a larger density depletion along the center of the O-mode beam, as might be expected to occur due to plasma heating not included in the model.

The typical shape of the field-aligned density rearrangement is illustrated in Fig. 7. This figure displays the z dependence of the ratio of the modified ion density to the cutoff density, n_i/n_c, along $x=30c/\omega_0$ in Fig. 6. The solid curves correspond to simulation results at different times (a) $\omega_0 t=520$, (b) $\omega_0 t=845$, and (c) $\omega_0 t=1300$. The dashed curve corresponds to the prediction of Eq. (6) and is seen to describe well the early development of cavity formation and the generation of "density wings." It is seen in Fig. 7 that, early in time, there are no locations along the z direction where a plasma resonance is encountered, i.e., along the field-line sampled the plasma is underdense. However, as time progresses, the magnitude of the "density wings" increases and eventually, as is indicated by curve (c), two resonant layers develop where $\omega_0=\omega_{pe}$. The axial density scale length of these nonlinear resonant layers is much smaller than the width, L, of the original O-mode beam. Thus they result in short-scale parallel electric fields that are responsible for the generation of the fast electron tails shown in Fig. 5.

To illustrate the development of the parallel electric fields $E_s(z,x,t)$ responsible for electron acceleration, it is useful to introduce a modulational description

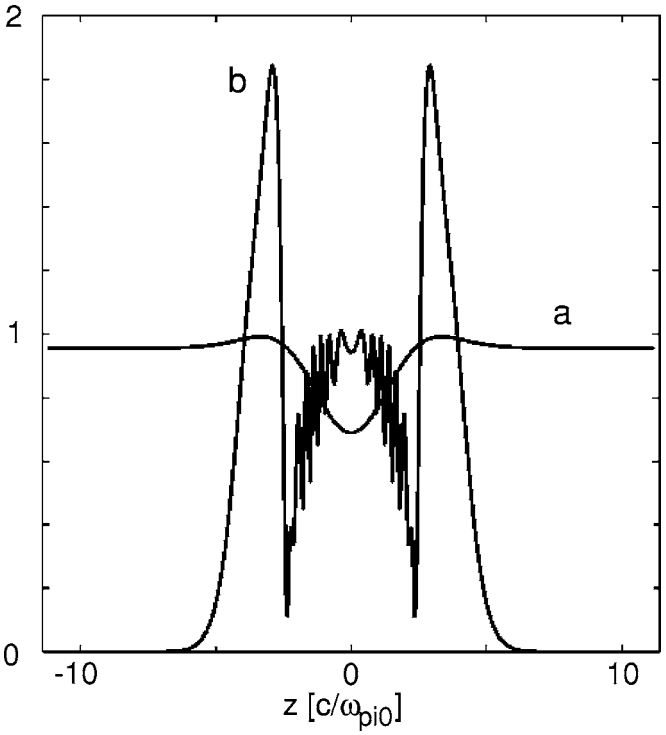

FIG. 8. Self-consistent formation of secondary electric fields predicted by Eqs. (6) and (10). Curve (a) is the scaled density n_i/n_c along an initially underdense field line. Curve (b) is the magnitude of the scaled, secondary electric field, $|A|/E_0$. At the peak of the density wings, where plasma resonance is matched, localized electric fields develop.

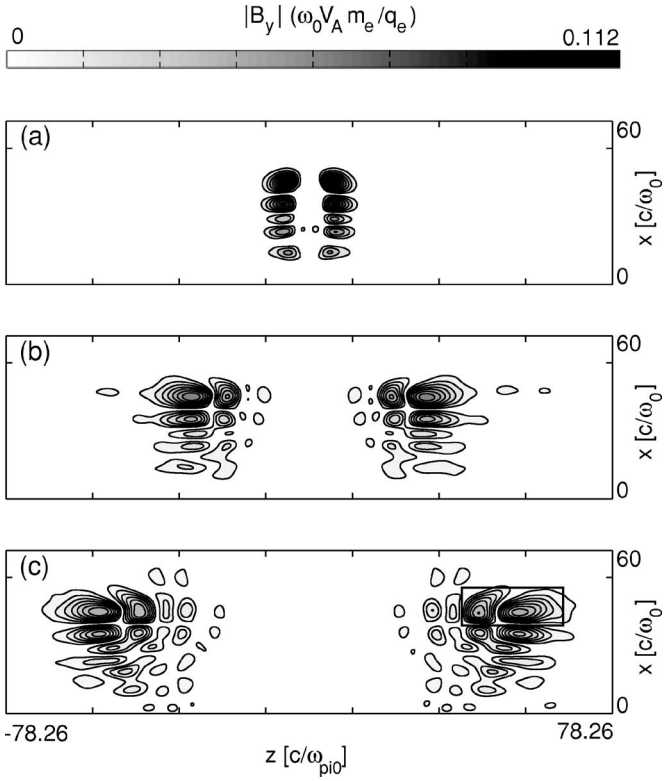

FIG. 9. Gray-scale contours showing time evolution of magnitude of B_y in the (x,z) plane with white the smallest value and black the largest. (a) $\omega_0 t=650$, (b) $\omega_0 t=1950$, and (c) $\omega_0 t=3250$. Two field-aligned pulses propagate away (i.e., $z>0$ and $z<0$) from the axial region illuminated by the O-mode signal. Propagating pulses are filamentary structures that originate at an x position corresponding to where a deep density cavity is formed. The rectangular region in (c) is sampled in Fig. 11.

$$E_s(z,x,t)=\frac{A(z,x,t)}{2}e^{-i\omega_0 t}+\text{c.c.}, \tag{9}$$

where A is a complex amplitude whose time dependence is considered slow compared to the frequency ω_0 of the primary field having amplitude $E_0h(x)g(z)$, which is constant in time. The amplitude A contains the short scale, resonantly driven fields generated by the density pileup, as well as the nonresonant modifications produced by the underdense cavities. The space-time evolution of these features is described by

$$2i\omega_0\frac{\partial}{\partial t}A+\left[\omega_0^2-\omega_{p0}^2\frac{n_i(z,x,t)}{n_0(x)}\right]A = \omega_{p0}^2[n_i(z,x,t)-n_0(x)]E_0h(x)g(z), \tag{10}$$

where ω_{p0} is the electron plasma frequency corresponding to the initial density n_0 at location x.

The early stage, self-consistent formation of the secondary electric fields is obtained by solving Eq. (10) together with Eq. (6). A typical pattern formed along a field line is illustrated in Fig. 8. The curve labeled (a) corresponds to the scaled, nonlinearly modified ion density, n_i/n_c, while the curve labeled (b) is the magnitude of the scaled, secondary electric field, $|A|/E_0$. It is seen that at the peak of the "density wings," where plasma resonance is matched, localized electric fields develop. These nonlinearly generated fields give rise to strong electron acceleration that results in the formation of field-aligned current channels emanating from the sides of a density cavity. It should be noted that at sufficiently large power levels, multiple streams of fast electrons can emanate from different x positions. The consequence of this feature is that independent Alfvénic filaments can be radiated by each of the resulting current channels. The fluid model discussed captures only the early stage of density cavity formation and the development of secondary resonant regions. Beyond this, kinetic processes develop that result in fast electron tails responsible for the excitation of shear Alfvén waves, as discussed next.

B. Alfvén waves

After the secondary electric fields arise and fast electron tails are generated, it is observed in the PIC simulation that electromagnetic signals develop, as seen in Fig. 9. These modes propagate along the confinement field at speeds much slower than the speed of light. The signals remain fairly collimated and have their magnetic field oriented in the shear polarization, i.e., B_y. These properties are consistent with radiated shear Alfvén modes. To fully illustrate these propagation characteristics, a color movie is required, but to convey a sense of the phenomena, Fig. 9 presents a series of snapshots in panels (a)–(c). They consist of gray-scale contours of the magnitude of B_y in the (x,z) plane with dark the largest value and white the smallest. Time increases sequentially from (a) $\omega_0 t=650$, (b) $\omega_0 t=1950$, to (c) $\omega_0 t=3250$. In comparing the patterns in Figs. 9(a)–9(c), it is seen that two

field-aligned pulses propagate away (i.e., $z>0$ and $z<0$) from the axial region previously illuminated by the O-mode signal. The propagating pulses are not plane waves across the magnetic field (x direction). Instead, they consist of filamentary structures. Each filament originates at an x position corresponding to where a deep density cavity is formed by the ponderomotive force. The reason is that currents are injected at these locations by the exiting fast electron tails. Each filament remains collimated within its corresponding Alfvén cone angle.[19,20] However, inside each filament the parallel wavelength varies as the pulses propagate away, in the characteristic fashion followed by finite-frequency shear modes. Detailed examination of the data leading to Fig. 9 reveals that the multiple Alfvénic filaments are embedded in a background of modes (not shown) that propagate isotropically and eventually scatter from the boundaries. These modes correspond to compressional (or fast) Alfvén waves. This behavior is consistent with results of a previous PIC-simulation study[18] in which it has been found that finite-size sources simultaneously radiate both polarizations of the Alfvénic disturbances.

Figure 10 illustrates further the characteristics of the magnetic field, B_y, of the filamentary shear modes traveling along the $\pm z$ directions in Fig. 9. Figure 10(a) displays the space-time signature (actually t vs z) of the signal at a fixed transverse position $x=40c/\omega_0$, near the unperturbed critical layer. This position corresponds to a magnetic field line that passes through a region (near $z\sim 0$) where secondary, resonant fields generate fast electrons. The value of B_y is represented by a gray scale, with white the largest positive value and black the largest negative. The sloping, small dashed line indicates the path followed by a signal moving at the zero-frequency, Alfvén speed v_A. It demonstrates that a significant portion of the collimated wave packet propagates nearly at this speed. In addition, it is seen that at late times (and larger z), the signals propagate at speeds that are progressively slower (indicated by the larger slope) than v_A. From a knowledge of the dispersion relation of finite-frequency shear Alfvén modes, it is expected that the slower, and thus late-arriving components of the wave packet have a frequency closer to the ion cyclotron frequency. Figure 10(b) shows the temporal signature sampled at a fixed z position, as indicated by the vertical, thick dashed line in Fig. 10(a). This trace is the equivalent of what a B-dot probe would measure in the laboratory. It shows that at early times the signal contains low frequencies. But as time progresses the frequency increases, as is expected for a packet of shear Alfvén waves. The continuous increase in frequency is also documented by the temporal evolution of the Wigner frequency distribution, $|W(t,\omega)|$, shown in Fig. 10(c).

Figure 11 provides insight into the self-consistent current system associated with the Alfvénic filaments that are excited by the fast electrons. Figure 11(a) displays small arrows corresponding to the local current-density vector at locations within the small region bounded by the rectangle superposed on Fig. 9(c). To aid the eye, a few "field lines" connecting the current vectors are drawn. They indicate the characteristic current-closure pattern of shear Alfvén waves; parallel electron currents are closed across the field by ion polariza-

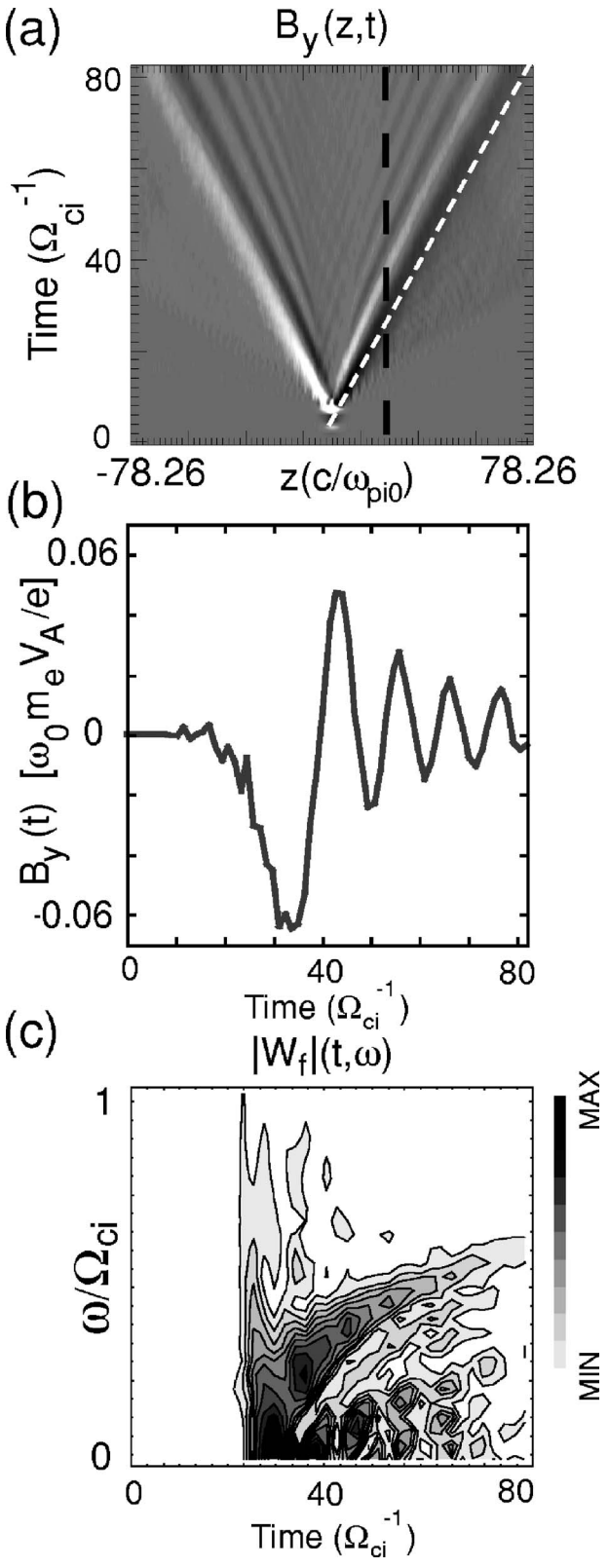

FIG. 10. Characteristics of the magnetic field, B_y, of the filamentary pulses traveling along the $\pm z$ directions in Fig. 9. (a) Space-time signature (scaled t vs z) of B_y at a fixed transverse position $x=40c/\omega_0$. B_y is represented by a gray scale, with white the largest positive value and black the largest negative. Sloping, small-dashed line indicates a signal moving at the Alfvén speed v_A. (b) Temporal signature at a fixed z position indicated by the vertical, thick dashed line in (a). (c) Wigner frequency distribution of B_y, $|W(t,\omega)|$, that shows an increase in frequency as time progresses.

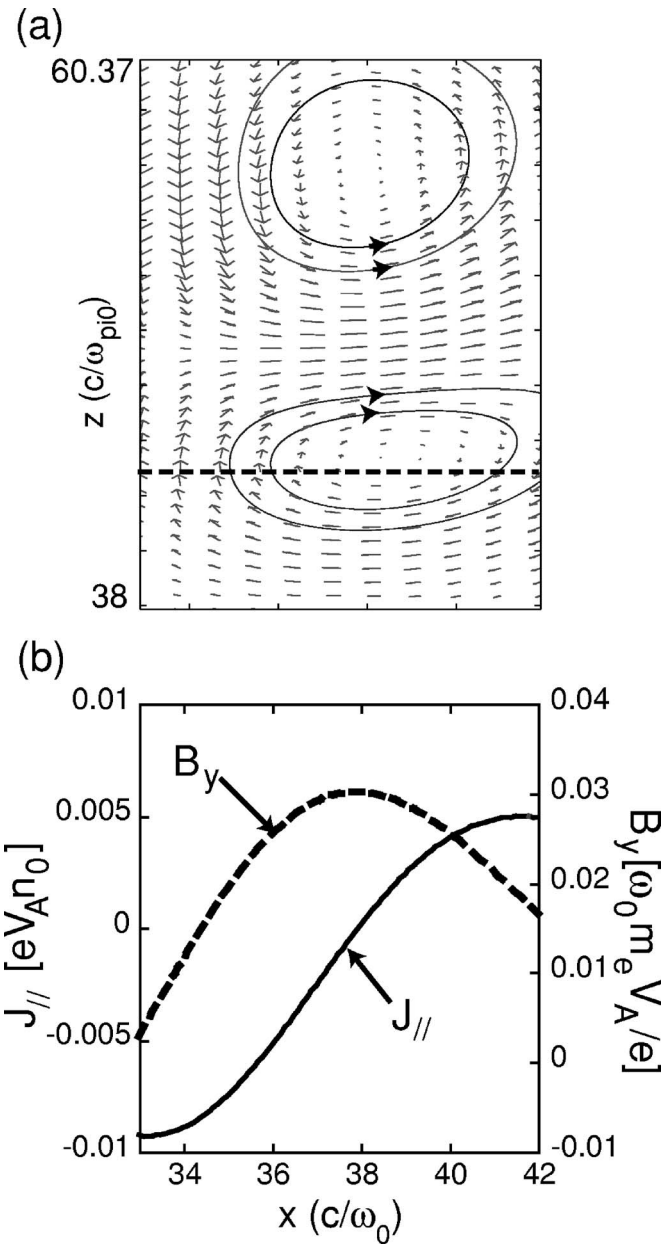

FIG. 11. Self-consistent current system of Alfvénic filaments. (a) Small arrows represent the local current-density vector within the small rectangle superposed on Fig. 10(c). A few "field lines" connecting the current-density vectors are drawn. The axial reversal in direction corresponds to the wavelength of the propagating pulse shown in Fig. 9(b). (b) Dashed curve is the component, B_y, of the magnetic field along the horizontal dashed line in (a). The solid curve is the parallel current along the same cut. It demonstrates that the filaments consist of coaxial structures.

tion currents. The axial reversal in direction of the current system corresponds to the wavelength of the propagating pulse whose temporal signature is given in Fig. 10(b). The dashed curve in Fig. 11(b) displays the x dependence of the y component, B_y, of the magnetic field associated with the Alfvénic filament sampled along a cut indicated by the horizontal dashed line in Fig. 11(a). The solid curve in Fig. 11(b) corresponds to the self-consistent parallel current along the same cut. It clearly demonstrates that the filaments consist of coaxial current structures.

IV. CONCLUSIONS

A kinetic (PIC) simulation complemented by a theoretical, fluid-based model has identified the nonlinear processes responsible for the excitation of shear Alfvén waves when a magnetized plasma is irradiated by a high-frequency pulse in the O-mode polarization. It has been found that the early stage of the interaction is dominated by the ponderomotive force produced by the primary fields of the pulse. This force pushes the cold plasma particles predominantly along the confinement magnetic field. As a consequence, density cavities are formed near the peaks of the nearly standing waveform of the pulse. The particles that are pushed out of the cavity region create field-aligned density increases, i.e., "density wings." At sufficiently large power levels, the increase in density results in new resonant layers where the frequency of the O-mode pulse matches the local value of the electron plasma frequency. What is significant about these secondary resonances is that they have short scale length and their density gradient lies along the direction of the primary electric field of the O-mode. This is in contrast with the linear behavior in which the O-mode matches the plasma resonance but results in wave reflection, and no absorption, because the density gradient is perpendicular to the electric field of the pulse.

Large-amplitude, localized electric fields arise at the secondary resonances. They cause electron heating and generate fast electron tails. The fast electrons that exit the "density wings" carry a field-aligned current of short transverse scale. The injected current induces a return current on the background plasma and forms a coaxial current system that is closed across the confinement field by ion-polarization currents. This collective response results in the excitation of shear Alfvén waves having a filamentary structure. The Alfvénic filaments emanate symmetrically out of the original footprint of the O-mode beam. As the power level is increased, multiple filaments appear along the various field lines that pass through a deep density cavity.

The radiated low-frequency pulses exhibit spatiotemporal patterns characteristic of finite-frequency Alfvén waves of small transverse scale. Each filament propagates with a group speed slightly slower than the Alfvén speed and spreads across the confinement magnetic field along a small cone angle. At a fixed position, the low frequencies in the wave packet arrive first and are followed by a train of oscillations of increasing frequency, but remain below the ion cyclotron frequency.

All the wave features and fast electron signatures described in the present study are consistent with detailed measurements made in a laboratory investigation.[14] However, the ponderomotive density modifications and the generation of secondary resonances isolated here have not yet been documented in the laboratory due to the technical difficulties associated with making probe measurements within the O-mode footprint. In this sense, the present study expands the perspective achieved in the laboratory and suggests that further measurements are required to map the microscopic origin of the Alfvénic signals. Indirectly, the observation that the laboratory study displays a power threshold for the gen-

eration of the Alfvénic signals is consistent with the requirement that the "density wings" be sufficiently large to permit the excitation of secondary resonances.

It should be mentioned that the laboratory study[14] has also considered the effect of *X*-mode polarization. Because the wave propagation characteristics for this polarization are significantly more involved, the simulation and modeling of such a situation requires a separate and dedicated investigation.

ACKNOWLEDGMENTS

The authors thank Dr. B. Van Compernolle and Professor W. Gekelman for many stimulating and insightful discussions concerning their experiment.

This work was sponsored by U.S. DOE Grant No. DE-FG02-03ER54717.

[1] A. J. Ferraro, H. S. Lee, R. Allhouse, K. Carroll, K. Lunnen, and T. Collins, J. Atmos. Terr. Phys. **46**, 855 (1984).
[2] K. Papadopoulos, K. Chang, P. Vitello, and A. Drobot, Radio Sci. **25**, 1311 (1990).
[3] R. Barr, Adv. Space Res. **21**, 677 (1998).
[4] For a perspective on recent developments, consult http://cmpd.umd.edu/
[5] K. Ko, C. R. Menyuk, A. Reiman, V. Tripathi, P. Palmadesso, and K. Papadopoulos, J. Geophys. Res. **91**, 10097 (1986).
[6] S. R. Lopes and A. C. Chian, Astron. Astrophys. **305**, 669 (1996).
[7] M. M. Shoucri, G. J. Morales, and J. E. Maggs, Phys. Fluids **28**, 2458 (1985).
[8] S. P. Kuo and M. C. Lee, Geophys. Res. Lett. **20**, 189 (1993).
[9] A. V. Strelsov, W. Lotko, and G. M. Milikh, J. Geophys. Res. **110**, 11 (2005).
[10] R. Barr and P. Stubbe, Geophys. Res. Lett. **18**, 1971 (1991).
[11] J. Villaseñor, A. Y. Wong, B. Song, J. Pau, M. McCarrick, and D. Sentman, Radio Sci. **31**, 211 (1996).
[12] G. M. Milikh, K. Papadopoulos, M. McCarrick, and J. Preston, Radiophys. Quantum Electron. **42**, 639 (1999).
[13] For an updated description of LAPD-U and BaPSF, consult http://plasma.physics.ucla.edu/bapsf/
[14] B. Van Compernolle, W. Gekelman, and P. Pribyl, Phys. Plasmas **13**, 092112 (2006).
[15] R. G. Hemker, Ph.D. thesis, UCLA (2000).
[16] F. S. Tsung, G. J. Morales, and J. N. Leboeuf, Phys. Rev. Lett. **90**, 055004 (2003).
[17] M. VanZeeland, W. Gekelman, S. Vincena, and G. Dimonte, Phys. Rev. Lett. **87**, 105001 (2001).
[18] F. S. Tsung, J. W. Tonge, and G. J. Morales, Phys. Plasmas **12**, 012508 (2005).
[19] W. Gekelman, D. Leneman, J. Maggs, and S. Vincena, Phys. Plasmas **1**, 3775 (1994).
[20] G. J. Morales, R. S. Loritsch, and J. E. Maggs, Phys. Plasmas **1**, 3765 (1994).
[21] G. J. Morales and Y. C. Lee, Phys. Rev. Lett. **33**, 1534 (1974).